AIMS Mathematics

AIMS Mathematics, 11(7): 20746–20772.
DOI: 10.3934/math.2026843
Received: 26 May 2026
Revised: 22 June 2026
Accepted: 30 June 2026
Published: 14 July 2026

https://www.aimspress.com/journal/Math

Research article

A state-switching PDE model for contact separation induced response amplification in girder bridges under bidirectional seismic excitation

Shutong Chen[1,2,*], Jieqin Liu[1], Leilei Li[1], Xuerong Liu[1], and Fuxing Ding[3]

[1] School of Intelligent Manufacturing and Construction, Jiangxi Polytechnic Institute (JPI), Xinyu 338000, China

[2] School of Civil Engineering, Universiti Sains Malaysia (USM), Engineering Campus, Nibong Tebal 14300, Malaysia

[3] School of Digital Industry, Jiangxi Metallurgical Vocational and Technical College, Xinyu 338000, China

* **Correspondence:** Email: chenshutong@student.usm.my.

Abstract: In this study, we develop a state-switching partial differential equation (PDE) model to investigate contact–separation-induced response amplification in girder bridges subjected to bidirectional seismic excitation. The girder and pier were idealized as Euler–Bernoulli beams, while the bearing was modeled as a Kelvin–Voigt element in the horizontal direction and a compression-only unilateral constraint in the vertical direction. A complementarity condition was introduced to describe the vertical girder–bearing interaction, and the horizontal transient response was formulated through state-dependent beam-type PDEs under contact and separation states. Based on modal expansion and state-switching conditions, a semi-analytical solution procedure was established to reveal the coupling mechanism between vertical contact loss and horizontal response amplification. Our numerical results showed that vertical excitation had a limited influence when continuous contact is maintained. However, when the excitation period approached the first vertical natural period, contact loss could occur and cause boundary-condition switching, leading to a significant increase in horizontal displacement. The dynamic V/H model produced stronger amplification than the fixed V/H assumption in the short-period range, while increasing span length further intensified the response. Local demand–capacity indicators, including the pier-base flexural demand ratio and the shear-key impact demand ratio, also increased when vertical excitation was considered. An OpenSees finite element (FE) comparison confirmed that the proposed analytical model could reasonably reproduce the main horizontal response characteristics. The proposed framework provides an effective reduced-order

approach for analyzing state-dependent bridge dynamics under bidirectional seismic excitation.

Keywords: state-switching model; PDE-based model; girder bridge; transient dynamic response; contact and separation; horizontal response
Mathematics Subject Classification: 74H45

1. Introduction

Mathematical modeling of transient structural dynamics with unilateral constraints is an important problem in applied mechanics and engineering mathematics. Bridge systems supported by bearings can be regarded as continuous dynamic systems whose vibration behavior is governed by coupled beam-type equations and boundary interaction conditions. Under strong bidirectional seismic excitation, the vertical component may reduce the contact force between the girder and the bearings to zero, leading to uplift, separation, and a sudden change in boundary constraints. As a result, the bridge response is no longer governed by a single linear vibration model, but by a state-switching system involving contact and separation states. The key mathematical challenge is therefore to formulate a model that can simultaneously describe the continuous vibration of the girder–bearing–pier system, the unilateral vertical contact condition, and the state-switching mechanism induced by bidirectional excitation.

Studies have shown that the dynamic response of bridge structures under near-field earthquakes differs markedly from that under conventional far-field excitation, and the effect of high-amplitude vertical ground motion cannot be neglected [1,2]. It is now widely recognized that this effect is closely related to the spectral-period characteristics, source-to-site distance and focal depth, and local site conditions. In the short-period range of near-field motions, the peak V/H ratio (defined as the ratio of vertical to horizontal ground-acceleration amplitudes) often significantly exceeds the conventional constant value of 2/3 [3–6]. As early as the beginning of the twentieth century, the influence of near-field vertical ground motion on structural systems had already been documented. At present, it is generally accepted that vertical seismic excitation may increase the axial force demand in bridge substructures [7–9], weaken the connection between the girder and the supporting substructure [4,10], and induce repeated impact between the superstructure and substructure [8,11]. For this reason, the role of vertical ground motion in bridge seismic analysis has attracted increasing attention in recent years.

Studies on the seismic response of bridges have mainly focused on numerical simulation, seismic performance assessment, and fragility analysis, whereas theoretical investigations based on continuum dynamics remain relatively limited. In contrast to discretized numerical approaches, continuum-based analysis takes the governing partial differential equations of structural dynamics as its starting point and is therefore better suited to revealing, in a direct manner, the interplay among wave propagation, boundary-constraint variation, and the intrinsic dynamic characteristics of the structure. In this context, the transient wave function expansion method, as a classical technique for solving the partial differential equations of elastodynamics, provides an important theoretical framework for deriving analytical representations of transient structural responses [12]. In early studies, St-Venant and Flamant, in turn, introduced stress-wave propagation theory into impact analysis and established the theory of planar bar impact, thus laying the foundation for subsequent theoretical and numerical studies of collision problems in bar-like structural systems [13]. Timoshenko et al. systematically investigated the forced vibration of rods and beams, thereby advancing the theoretical development of the governing equations for continuum structural dynamics [14]. Subsequently, Tian and Yin performed a transient analysis of the repeated impact process in flexible bars based on the aforementioned theoretical framework [15]. For bridge structures, Xu and Yin employed the transient wave eigenfunction expansion method to idealize a girder bridge as a coupled beam–bar continuum system, on the basis of which the vertical dynamic response of the structure was analyzed [16,17]. On this basis, Yang et al. further developed a beam–spring–bar model to investigate the dynamic response and internal-force evolution of bridges under vertical seismic excitation [18,19]. An et al. then employed this approach to examine the influence of vertical ground motion on the longitudinal dynamic response of bridge piers [20,21]. These studies indicate that continuum modeling and analytical approaches based on partial differential equations possess considerable theoretical potential for transient dynamic analysis of bridges. However, researchers has focused predominantly on vertical or longitudinal responses, with insufficient attention given to the horizontal secondary effects induced by girder–bearing separation under near-field earthquakes. In particular, there is a lack of a unified continuum partial-differential-equation model for bridges that simultaneously incorporates horizontal seismic excitation, contact–separation state switching, and multi-source input characteristics. Especially under near-field multi-source seismic input, bidirectional partial-differential-equation modeling and analytical investigation for horizontal bridge systems remain limited.

Compared with beam–bar or beam–spring–bar continuum models that mainly focused on vertical vibration, longitudinal response, or internal-force evolution of bridge systems, we extend the PDE-based framework to the horizontal dynamic response induced by vertical contact loss. The main advancement of the proposed model lies in the explicit incorporation of the contact–separation state transition into the horizontal governing equations. In this formulation, vertical contact loss is not treated only as a local support response, but as a switching variable that changes the effective horizontal boundary conditions of the girder–bearing–pier system. Therefore, the proposed model provides a state-dependent continuum formulation for revealing how vertical separation can amplify horizontal displacement, pier-base flexural demand, and shear-key impact demand under bidirectional seismic excitation. To address this issue, we develop a state-switching PDE model for the horizontal response of a girder–bearing–pier system subjected to near-field bidirectional seismic excitation. The proposed model distinguishes two structural states, namely girder–bearing contact and separation, and formulates the corresponding governing equations, boundary conditions, and displacement–velocity continuity conditions within a continuum dynamics framework. By using wave-function expansion, modal superposition, and the Duhamel integral, semi-analytical solutions are obtained for the horizontal vibration response and the shear-key impact demand. The formulation is then used to clarify how vertical contact loss changes the effective boundary constraints of the system and amplifies horizontal displacement, pier-base flexural demand, and shear-key impact demand. In addition, a simplified OpenSees FE model is established to verify the horizontal dynamic response predicted by the proposed analytical formulation.

2. Mathematical formulation of the girder–bearing–pier system

2.1. Basic assumptions

A principal advantage of theoretical analysis lies in its decoupling capability, which can substantially reduce the interference of seismic randomness in identifying the underlying response mechanisms. Figure 1 shows the theoretical model adopted in this study. To capture the primary structural response behavior, the structure is simplified as follows:

(1) As the horizontal seismic response is mainly governed by flexural deformation, the girder and pier are idealized as *Euler–Bernoulli* beams in the horizontal direction, and shear deformation and torsion are therefore neglected.
(2) Considering that laminated rubber bearings provide horizontal stiffness and damping but cannot resist tension during uplift, the bearing is modeled as a Kelvin–Voigt element in the horizontal direction and as a compression-only unilateral constraint in the vertical direction.
(3) To focus on the coupling mechanism between vertical contact loss and horizontal response amplification, the horizontal and vertical ground motions are assumed to act uniformly on the bridge system. They are applied synchronously in the basic analysis, while arrival-time differences are considered separately in parametric study; traveling-wave effects are neglected.
(4) Since the main concern is the dynamic effect induced by contact–separation rather than material energy dissipation, the intrinsic damping of reinforced concrete is neglected. Only the viscous damping of the *Kelvin–Voigt* bearing is retained in the analytical model.

These assumptions are adopted to maintain the analytical tractability of the proposed reduced-order PDE model and to focus on the dominant contact–separation-induced amplification mechanism. Therefore, the model is mainly applicable to slender girder–pier systems dominated by flexural deformation, while shear deformation, torsional effects, intrinsic concrete damping, and detailed high-frequency re-contact impact behavior are not explicitly considered. These simplifications may influence the local response amplitude but do not affect the main mechanism discussed in this study. More refined modeling of damping, shear–torsion coupling, material nonlinearity, and re-contact effects can be considered in future work.

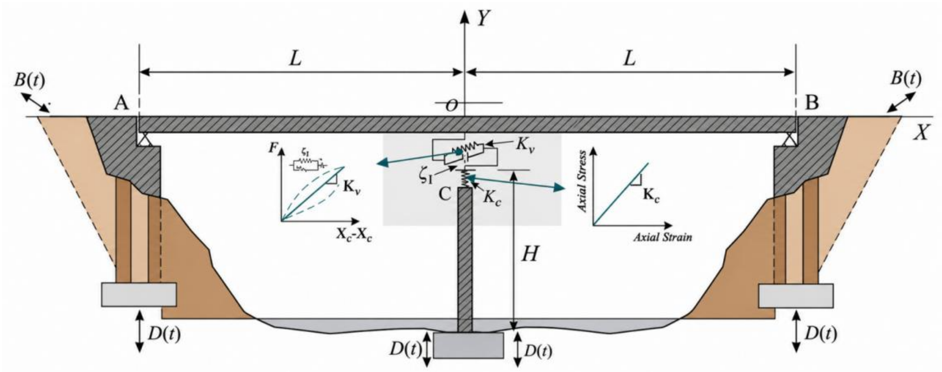

Figure 1. Theoretical computational model.

2.2. Unilateral contact condition

In this model, the horizontal response is considered under two conditions, namely vertical contact and vertical separation between the girder and the bearing. The detailed governing equations and derivation of the vertical dynamic response can be found in [18,19] and are therefore omitted here.

In the vertical direction, the bearing is assumed to resist compression but not tension. Therefore, the interaction between the girder and the bearing is described by a unilateral contact condition rather than a bilateral displacement constraint. Let g(t) denote the vertical gap between the girder and the bearing, and let N(t) denote the vertical contact force transmitted through the bearing. The gap is taken to be non-negative, with g(t)=0 representing closed contact and g(t)>0 representing separation. The unilateral contact law can then be written in the following complementarity form:

$$\mathrm{g}(t) \geq 0,\ N(t) \geq 0,\ \mathrm{g}(t)N(t) = 0\ . \tag{1}$$

This condition states that the girder and the bearing cannot penetrate each other, the bearing can only provide only compressive contact force, and the vertical gap and contact force cannot be positive at the same time. Therefore, two admissible structural states can be distinguished. When g(t)=0,N(t)>0, the girder and the bearing remain in contact, and the bearing provides vertical support to the girder. In this case, the horizontal response of the girder–bearing–pier system is governed by the contact-state dynamic model, in which the girder and pier are coupled through the bearing constraint.

By contrast, when g(t)>0,N(t)=0, vertical separation occurs, and the bearing no longer transmits vertical contact force. The girder and the substructure then vibrate independently in the vertical direction, and the horizontal boundary conditions of the system are modified accordingly.

For this bridge system, the first separation time is defined as:

$$t_1 = \inf\left\{t>0 \middle| N(t)=0, g(t) \geq 0\right\}, \tag{2}$$

where t_1 denotes the instant at which the vertical contact force first vanishes. At this instant, the horizontal displacement and velocity of the system are assumed to remain continuous.

In the following subsections, the horizontal governing equations are therefore derived separately for the contact and separation phases (Figure 2), and the above complementarity condition is used to determine the active structural state.

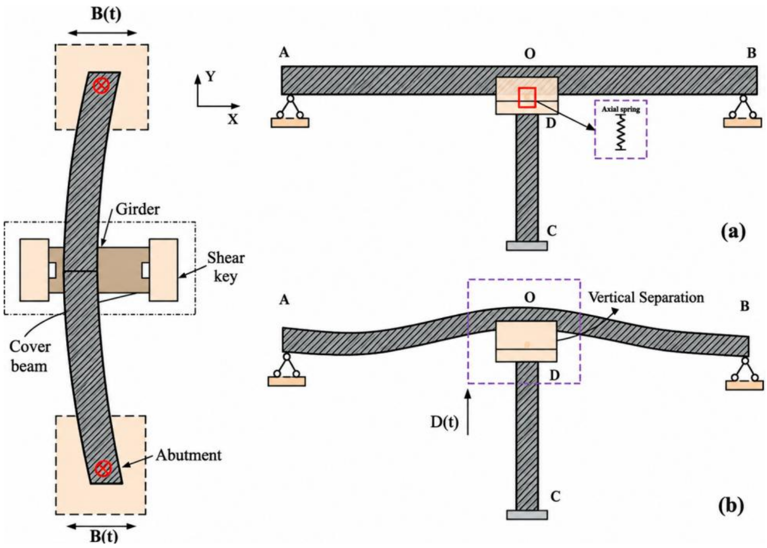

Figure 2. Two states in horizontal dynamic analysis of bridges (a: vertical contact state; b: vertical separation state).

2.3. Contact-state governing equations

During the vertical contact phase, the governing horizontal bending-wave equations for the girder segments OA and OB and the pier segment CD are expressed as follows:

$$\begin{aligned}
&OA: E_b I_{bx}\frac{\partial^4 X_1(x,t)}{\partial x^4}+\rho_b A_b\frac{\partial^2 X_1(x,t)}{\partial t^2}=0\\
&OB: E_b I_{bx}\frac{\partial^4 X_2(x,t)}{\partial x^4}+\rho_b A_b\frac{\partial^2 X_2(x,t)}{\partial t^2}=0\\
&CD: \frac{E_c I_c\partial^4 X_c(\xi,t)}{\partial \xi^4}+\rho_b A_c\frac{\partial^2 X_c(\xi,t)}{\partial t^2}=0
\end{aligned}\quad, \tag{3}$$

where the displacement of the girder–pier system is decomposed into three components, namely, the static component $X_s(x)$, the rigid-body component $X_g(x,t)$, and the dynamic component $X_d(x,t)$:

$$\begin{aligned}
&X_1(x,t)=X_{1s}(x)+X_{1g}(x,t)+X_{1d}(x,t)\\
&X_1(x,t)=X_{1s}(x)+X_{1g}(x,t)+X_{1d}(x,t)\\
&X_c(\xi,t)=X_{cs}(\xi)+X_{cg}(\xi,t)+X_{cd}(\xi,t)
\end{aligned}\quad. \tag{4}$$

In the initial state, the static and rigid-body displacements of the girder and piers satisfy:

$$\begin{aligned}
&X_{1s}(x)=X_{2s}(x)=X_{cs}(x)=0\\
&X_{1g}(x,t)=X_{2g}(x,t)=X_{cg}(\xi,t)=D(t)
\end{aligned}. \tag{5}$$

Substituting the conditions from Eqs (4) and (5) into Eq (3) yields:

$$\begin{aligned}
&OA: E_b I_b\frac{\partial^4 X_{1d}(x,t)}{\partial x^4}+\rho A_b\frac{\partial^2 X_{1d}(x,t)}{\partial t^2}=-\rho_b A_b\frac{\partial^2 X_{1g}(x,t)}{\partial t^2}\\
&OB: E_b I_b\frac{\partial^4 X_{2d}(x,t)}{\partial x^4}+\rho A_b\frac{\partial^2 X_{2d}(x,t)}{\partial t^2}=-\rho_b A_b\frac{\partial^2 X_{2g}(x,t)}{\partial t^2}\\
&CD: E_c I_c\frac{\partial^4 X_{cd}(\xi,t)}{\partial \xi^4}+\rho_c A_c\frac{\partial^2 X_{cd}(\xi,t)}{\partial t^2}=-\rho_c A_c\frac{\partial^2 X_{cg}(\xi,t)}{\partial t^2}
\end{aligned}\quad. \tag{6}$$

Equation (6) is a non-homogeneous differential equation concerning the transient displacement response X_d of the girder and piers. To construct the solution, the associated homogeneous problem is first considered:

$$\begin{aligned}
&OA: a_x^2\frac{\partial^4 X_{1d}(x,t)}{\partial x^4}+\frac{\partial^2 X_{1d}(x,t)}{\partial t^2}=0\\
&OB: a_x^2\frac{\partial^4 X_{2d}(x,t)}{\partial x^4}+\frac{\partial^2 X_{2d}(x,t)}{\partial t^2}=0\\
&CD: c_1^2\frac{\partial^4 X_{cd}(\xi,t)}{\partial \xi^4}+\frac{\partial^2 X_{cd}(\xi,t)}{\partial t^2}=0
\end{aligned}\,, \tag{7}$$

where a_x*, c_1 are the* horizontal wave vibration parameters for the girder and piers, respectively, and satisfy: $a_x=\sqrt{E_b I_{bx}/\rho_b A_b}$, $c_1=\sqrt{E_c I_c/\rho_c A_c}$.

To solve the governing equations, a time-harmonic ansatz is introduced, and the dynamic responses of the bridge system are assumed to be of the form $X_{1d}(x,t)=e^{i\omega_i t}\varphi_{i1}(x)$, $X_{2d}(x,t)=e^{i\omega_i t}\varphi_{i2}(x)$, $X_{cd}(\xi,t)=e^{i\omega_i t}\varphi_{ic}(\xi)$, and substituting these expression into Eq (7) yields:

$$\begin{aligned} {a_x}^2{\varphi_{i1}}^{(4)} - {\omega_i}^2\varphi_{i1} = 0 \\ {a_x}^2{\varphi_{i2}}^{(4)} - {\omega_i}^2\varphi_{i2} = 0 \\ {c_1}^2{\varphi_{ic}}^{(4)} - {\omega_i}^2\varphi_{ic} = 0 \end{aligned} , \tag{8}$$

where ω_i is the ith horizontal natural circular frequency of the composite system, and the corresponding flexural mode shapes of the girder and the pier are given by:

$$\begin{aligned} \varphi_{i1}(x) = A_1 \sin K_{ib}x + B_1 \cos K_{ib}x + C_1 \sinh K_{ib}x + D_1 \cosh K_{ib}x \\ \varphi_{i2}(x) = A_2 \sin K_{ib}x + B_2 \cos K_{ib}x + C_2 \sinh K_{ib}x + D_2 \cosh K_{ib}x \\ \varphi_{ic}(\xi) = E_1 \sin K_{ic}\xi + F_1 \cos K_{ic}\xi + G_1 \sinh K_{ic}\xi + H_1 \cosh K_{ic}\xi \end{aligned} , \tag{9}$$

where $A_1 \sim D_2, E_1 \sim H_1$ denote the undetermined coefficients associated with the flexural-wave mode functions of the girder and the pier. Here, k_{ib} and k_{ic} are the corresponding wave numbers, and the frequency–wave-number relations are given by $K_{ib} = \sqrt{\omega_i / a_x}$, $K_{ic} = \sqrt{\omega_i / c_1}$. For the symmetric horizontal vibration modes of the composite structure about the mid-span of the girder, the corresponding mode shapes are required to satisfy the following boundary and continuity conditions:

$$\begin{aligned} \varphi_{i1}(-L) = 0, \varphi''_{i1}(-L) = 0 \\ \varphi_{i2}(L) = 0, \varphi''_{i2}(L) = 0, \\ \varphi_{i1}(0) = \varphi_{i2}(0), \quad \varphi'_{i1}(0) = \varphi'_{i2}(0), \quad \varphi''_{i1}(0) = \varphi''_{i2}(0) \\ \varphi_{ic}(0) = 0, \varphi'_{ic}(0) = 0 \end{aligned} \tag{10}$$

$$\begin{aligned} \varphi_{ic}(H) = \varphi_{i1}(0) + \frac{E_c I_c \varphi'''_{ic}(H)}{K_v} \\ E_b I_b(\varphi'''_{i1}(0) - \varphi'''_{i2}(0)) - E_c I_c \varphi'''_{ic}(H) = -\omega_i^2 M_a \varphi_{ic}(H) \end{aligned} . \tag{11}$$

By enforcing the boundary and continuity conditions, a homogeneous linear algebraic system for the undetermined coefficients is obtained, and the corresponding characteristic equation follows from the condition of nontrivial solvability.
Substituting conditions (10) and (11) into Eq (9) yields:

$$\begin{aligned} \varphi_{i1}(x) = E_i\left(-\frac{\sin K_{ib}(x+L)}{\cos K_{ib}L} + \frac{shK_{ib}(x+L)}{chK_{ib}L}\right) \\ \varphi_{i2}(x) = E_i\left(\frac{\sin K_{ib}(x-L)}{\cos K_{ib}L} - \frac{shK_{ib}(x-L)}{chK_{ib}L}\right) \\ \varphi_{ic}(\xi) = E_i\left[M_2(\sin K_{ic}\xi - shK_{ic}\xi) + M_3(\cos K_{ic}\xi - chK_{ic}\xi)\right] \end{aligned} . \tag{12}$$

The undamped natural frequencies of the composite system are determined from the following equation:

$$\begin{aligned} M_2(\sin K_{ic}H - shK_{ic}H) + M_3(\cos K_{ic}H - chK_{ic}H) \\ = (\tan K_{ib}L - thK_{ib}L) + 4E_b I_b K_{ib}^3 / K_v \end{aligned} \tag{13}$$

where M_a denotes the lumped mass of the cap beam, and K_v is the transverse shear stiffness of the bearing.

Since the damping is assumed to be small and mainly localized in the bearing, the undamped mode shapes are adopted as the expansion basis, while the bearing damping is incorporated into the generalized modal equations through modal projection. Within the framework of the wave-function expansion method, the dynamic term of the structure is represented as a series expansion in terms of modal functions:

$$\begin{gathered} X_{1d}=\sum_{i=1}^{\infty}\varphi_{i1}(x)q_i(t), X_{2d}=\sum_{i=1}^{\infty}\varphi_{i2}(x)q_i(t) \\ X_{cd}=\sum_{i=1}^{\infty}\varphi_{ic}(\xi)q_i(t) \end{gathered} . \tag{14}$$

The wave equation is thereby reduced to an ordinary differential equation with respect to the time-dependent function q_i(t):

$$\ddot{q}_i(t)+\omega_i^2 q_i(t)+2\zeta_1\omega_i\dot{q}_i(t)=\ddot{Q}_i(t) \tag{15}$$

where ζ_1 denotes the damping coefficient of the bearing, and $Q_i(t)$ is the generalized force corresponding to the i-th mode, satisfying:

$$\ddot{Q}_i(t)=-\int_{-L}^{0}\rho_b A_b\ddot{X}_{1g}(x,t)\varphi_{i1}(x)dx-\int_0^L\rho_b A_b\ddot{X}_{2g}(x,t)\varphi_{i2}(x)dx-\int_0^H\rho_c A_c\ddot{X}_g(\xi,t)\varphi_{ic}(\xi)d\xi . \tag{16}$$

Under the prescribed initial conditions, by means of the Laplace transform, the time-dependent function $q_i(t)$ for the bridge structure can be derived as follows:

$$q_i(t)=e^{-\zeta_1\omega_i t}\left(q_i(0)\cos\omega_d t+\frac{\dot{q}_i(0)+\omega_i\zeta_1 q_i(0)}{\omega_d}\sin\omega_d t\right)+\frac{1}{\omega_d}\int_0^t e^{-\zeta_1\omega_i t}\ddot{Q}_i(\tau)\sin\omega_d(t-\tau)d\tau \tag{17}$$

where ω_d represents the damp natural frequency of the structure, satisfying $\omega_d=\omega_i\sqrt{1-\zeta_1^2}$.

At the initial time, the structure is at rest, and the following initial conditions are imposed:

$$q_i(0)=0,\dot{q}_i(0)=0 \tag{18}$$

Under the contact state, the dynamic response functions of the composite structure at the mid-span of the girder and the top of the pier are given by:

$$\begin{gathered} X_{1d}(0,t)=-\frac{1}{\omega_d}\sum_{i=1}^{\infty}\varphi_{i1}(0)\int_0^t e^{-\zeta_1\omega_i t}\ddot{Q}_i(\tau)\sin\omega_d(t-\tau)d\tau \\ X_{2d}(0,t)=-\frac{1}{\omega_d}\sum_{i=1}^{\infty}\varphi_{i2}(0)\int_0^t e^{-\zeta_1\omega_i t}\ddot{Q}_i(\tau)\sin\omega_d(t-\tau)d\tau \\ X_{cd}(H,t)=-\frac{1}{\omega_d}\sum_{i=1}^{\infty}\varphi_{ic}(H)\int_0^t e^{-\zeta_1\omega_i t}\ddot{Q}_i(\tau)\sin\omega_d(t-\tau)d\tau \end{gathered} . \tag{19}$$

2.4. Separation-state governing equations

After vertical separation occurs between the girder and the bearing, the girder and the pier system move independently. In this case, the governing wave equations for the girder and the pier are given by:

$$
\begin{aligned}
&AB: E_b I_{bx} \frac{\partial^4 \bar{X}_b(x,t)}{\partial x^4} + \rho_b A_b \frac{\partial^2 \bar{X}_b(x,t)}{\partial t^2} = 0 \\
&CD: \frac{E_c I_c \partial^4 \bar{X}_c(\xi,t)}{\partial \xi^4} + \rho_b A_c \frac{\partial^2 \bar{X}_c(\xi,t)}{\partial t^2} = 0
\end{aligned}
\quad . \tag{20}
$$

Following the procedure presented in Section 2.1, the dynamic displacement responses of the girder and the pier can be expressed as follows:

$$
\begin{aligned}
&a_x{}^2 \bar{\varphi}_i{}^{(4)} - \omega_{ib}{}^2 \bar{\varphi}_i = 0 \\
&c_1{}^2 \bar{\varphi}_{ic}{}^{(4)} - \omega_{ic}{}^2 \bar{\varphi}_{ic} = 0
\end{aligned}
\quad . \tag{21}
$$

In this state, the girder and the bearing are detached and no longer interact with each other; accordingly, the structural mode shapes are required to satisfy the following boundary conditions:

$$
\begin{aligned}
&\bar{\varphi}_i(-L,t) = \bar{\varphi}_i(L,t) = 0, \frac{\partial^2 \bar{\varphi}_i(-L,t)}{\partial x^2} = \frac{\partial^2 \bar{\varphi}_i(L,t)}{\partial x^2} = 0 \\
&\bar{\varphi}_{ic}(0,t) = \frac{\partial \bar{\varphi}_{ic}(0,t)}{\partial \xi} = 0, E_c I_c \frac{\partial^2 \bar{\varphi}_{ic}(0,t)}{\partial \xi^2} = 0 \\
&E_c I_c \frac{\partial^3 \bar{\varphi}_{ic}(H,t)}{\partial \xi^3} = M_a \frac{\partial^2 \bar{\varphi}_{ic}(H,t)}{\partial t^2}
\end{aligned}
\tag{22}
$$

where ω_{ib} and ω_{ic} are the horizontal natural circular frequency of the girder and pier, respectively， The flexural mode functions for each mode can be expressed as follows:

$$
\begin{aligned}
&\bar{\varphi}_i(x) = A_3 \sin \bar{K}_{ib} x + B_3 \cos \bar{K}_{ib} x + C_3 \sinh \bar{K}_{ib} x + D_3 \cosh \bar{K}_{ib} x \\
&\bar{\varphi}_{ic}(\xi) = E_3 \sin \bar{K}_{ic} \xi + F_3 \cos \bar{K}_{ic} \xi + G_3 \sinh \bar{K}_{ic} \xi + H_3 \cosh \bar{K}_{ic} \xi
\end{aligned}
\quad . \tag{23}
$$

where $A_3 \sim D_3, E_3 \sim H_3$ denote the undetermined coefficients associated with the flexural-wave mode functions of the girder and the pier in this state.

Substituting the boundary conditions into the modal function yields:

$$
\begin{aligned}
&\bar{\varphi}_i(x) = \bar{A}_i \sin \bar{K}_{ib}(x+L) \\
&\bar{\varphi}_{ic}(\xi) = \bar{E}_{i2} \left(\sin \bar{K}_{ic} \xi - \sinh \bar{K}_{ic} \xi - \frac{\sin \bar{K}_{ic} H + sh \bar{K}_{ic} H}{\cos \bar{K}_{ic} H + ch \bar{K}_{ic} H} (\cos \bar{K}_{ic} \xi - ch \bar{K}_{ic} \xi) \right)
\end{aligned}
\tag{24}
$$

where $\bar{K}_{ib}$ and $\bar{K}_{ic}$ denote the wave numbers associated with separation state, satisfying the following relation $\bar{K}_{ib} = \sqrt{\omega_{ib} / a_x}$, $\bar{K}_{ic} = \sqrt{\omega_{ic} / c_1}$.

The eigenfrequency equations for the girder ω_{ib} and the pier ω_{ic} are obtained as:

$$
\begin{aligned}
&\omega_{ib} = \sqrt{\frac{E_b I_{bx}}{\rho_b A_b}} \cdot \frac{i^2 \pi^2}{4L^2} \\
&\omega_{ic} = \sqrt{\frac{E_c I_c \bar{K}_{ic}^3 (1 + \cos \bar{K}_{ic} H \cdot ch \bar{K}_{ic} H)}{M_a (\cos \bar{K}_{ic} H \cdot sh \bar{K}_{ic} H - \sin \bar{K}_{ic} H \cdot ch \bar{K}_{ic} H)}}
\end{aligned}
\quad . \tag{25}
$$

Similarly, based on the orthogonality conditions of the structure, the time functions $q_{ib}(t)$and $q_{ic}(t)$ associated with the girder and the pier, respectively, are governed by:

$$\begin{aligned} q_{ib}(t^*) &= q_{ib}(t_1)\cos\omega_{ib}t^* + \frac{\dot{q}_{ib}(t_1)}{\omega_{ib}}\cos\omega_{ib}t^* + \frac{1}{\omega_{ib}}\int_0^{t^*}\ddot{Q}_{ib}(t_1+\tau)\sin\omega_{ib}(t^*-\tau)d\tau \\ q_{ic}(t^*) &= q_{ic}(t_1)\cos\omega_{ic}t^* + \frac{\dot{q}_{ic}(t_1)}{\omega_{ic}}\cos\omega_{ic}t^* + \frac{1}{\omega_{ic}}\int_0^{t^*}\ddot{Q}_{ic}(t_1+\tau)\sin\omega_{ic}(t^*-\tau)d\tau \end{aligned} \tag{26}$$

where t_1 denotes the instant of the first separation time, and $t^*=t\text{-}t_1$ represents the elapsed time in the separation phase. Considering that the restraint during the possible re-contact process after separation is relatively weak and its duration is short, it is therefore assumed that, after the first separation, the girder and the substructure undergo free vibration independently according to their respective intrinsic dynamic characteristics, ω_{ib}, ω_{ic}.

At the switching instant t_1, no impulsive horizontal force is assumed to act directly on the girder–bearing interface. Therefore, the horizontal displacement and velocity should remain continuous across the transition. The continuity conditions are expressed as:

$$\begin{aligned} \bar{X}_b(0,t_1) = X_1(0,t_1),\ \dot{\bar{X}}_b(0,t_1) = \dot{X}_1(0,t_1) \\ \bar{X}_c(H,t_1) = X_c(H,t_1),\ \dot{\bar{X}}_c(H,t_1) = \dot{X}_c(H,t_1) \end{aligned}. \tag{27}$$

Based on these continuity conditions, the initial generalized time functions of the separated girder and pier can be obtained by projecting the displacement and velocity fields at t_1 onto their corresponding modal functions. Thus,

$$\begin{aligned} q_{ib}(t_1) &= \bar{\varphi}_{ib}\left(\rho_b A_b\int_{-L}^{0}X_1(x,t_1)dx + \rho_b A_b\int_0^L X_2(x,t_1)dx\right) \\ \dot{q}_{ib}(t_1) &= \bar{\varphi}_{ib}\left(\rho_b A_b\int_{-L}^{0}\dot{X}_1(x,t_1)dx + \rho_b A_b\int_0^L \dot{X}_2(x,t_1)dx\right) \\ q_{ic}(t_1) &= \bar{\varphi}_{ic}\left(\rho_c A_c\int_0^H X_c(\xi,t_1)d\xi\right) \\ \dot{q}_{ic}(t_1) &= \bar{\varphi}_{ic}\left(\rho_c A_c\int_0^H \dot{X}_c(\xi,t_1)d\xi\right) \end{aligned}. \tag{28}$$

2.5. Qualitative interpretation of the state-switching model

The above formulation indicates that the girder–bearing–pier system is governed by a state-switching model rather than a single linear vibration model. The vertical contact force acts as the switching variable: When contact is maintained, the girder and pier remain coupled through the bearing constraint; after separation, the effective boundary conditions change, and the two components vibrate according to the separation-state equations.

For each prescribed state, the governing equations are linear deterministic beam-type equations, and the modal response remains bounded under bounded excitation away from resonance. However, when the excitation period approaches the structural natural period, resonance-like amplification may occur. The displacement and velocity continuity conditions at the switching instant ensure that the contact–separation transition does not introduce nonphysical jumps, but changes the subsequent dynamic evolution through boundary-condition switching.

3. Numerical implementation and dynamic response profiles

The numerical model adopted in this study is based on a two-span elevated girder bridge. The girder has a box-section configuration, with the following equivalent properties: the density of reinforced concrete is taken as 2600 kg/m³; an equivalent Young's modulus of E_b=12.1Gpa, an equivalent composite cross-sectional area of $A_b \approx 6.3\ \mathrm{m}^2$accounting for reinforcement and concrete, and a horizontal equivalent moment of inertia of $I_{bx} \approx 38\ \mathrm{m}^4$. The girder is connected to the cap beam through laminated rubber bearings, which are assumed to resist compression only and not tension. The horizontal stiffness K_v and vertical stiffness K_c of the bearings are 2×10^9 N/m and 2×10^6 N/m, respectively, and their damping effect is also considered $\xi = 2\%$. The bridge piers are designed as prismatic circular-section piers, with an equivalent elastic modulus of approximately E_c=30 GPa and an equivalent cross-sectional area of approximately 3.09 m². The shear keys adopt an integral external configuration, with cushioning rubber pads embedded between the main girder and the shear keys. The compressive stiffness of the rubber pads is $K_p = 2\times10^8$ N/m. The reinforcement details of the bridge piers and shear keys are illustrated in Figure 3.

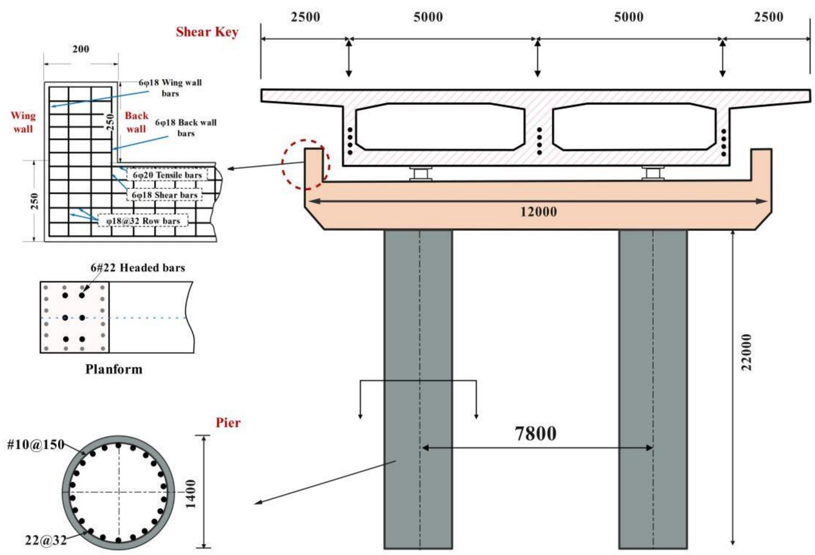

Figure 3. Parameters of bridge structures.

In seismic engineering research, ground motion inputs are commonly represented by either real earthquake records or artificial harmonic excitations. In this study, artificial harmonic excitations are adopted to isolate the effects of excitation period and amplitude on the contact–separation-induced amplification mechanism, rather than to reproduce the full randomness of real earthquake records. Although harmonic excitations cannot fully capture the nonstationary characteristics, multi-frequency contents, pulse effects, duration effects, and record-to-record variability of real near-field ground motions, they provide a controllable input condition for identifying and capturing the dominant relationship between vertical contact loss and horizontal response amplification. Therefore, our results should be interpreted as mechanism-oriented analytical findings under simplified near-field-relevant excitation conditions, and further studies will incorporate real near-field earthquake records to verify and extend the applicability of the proposed state-switching PDE model.

To fully account for the influence of near-field vertical seismic characteristics, the seismic input is simplified as decoupled harmonic excitations in the horizontal and vertical directions, denoted by $D(t)$ and $B(t)$, respectively. The initial horizontal excitation amplitude α_H is set to 0.5g (510gal). In accordance with common engineering practice, the first five structural modes are retained in the modal analysis. Figure 4 summarizes the complete state-switching solution procedure: The vertical contact condition determines the active structural state, the corresponding horizontal equations are solved, and the key response quantities are extracted for parametric and demand-to-capacity analyses.

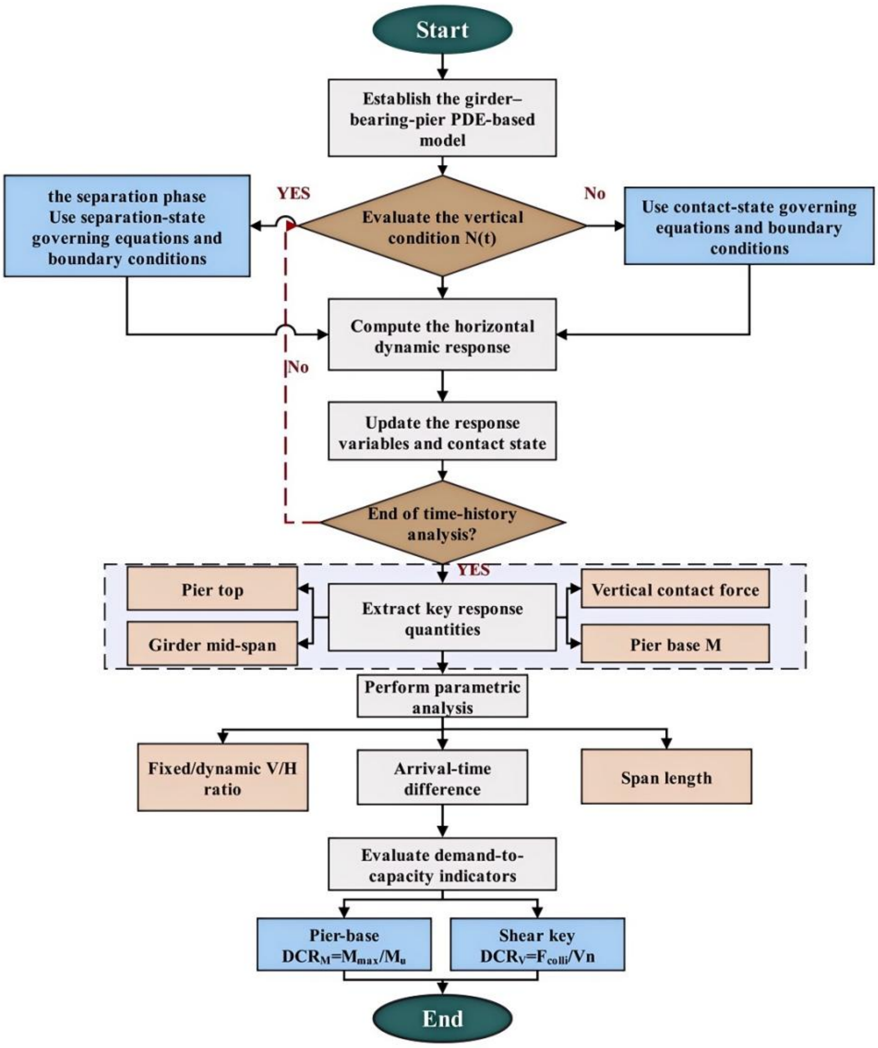

Figure 4. Flowchart of the state-switching semi-analytical solution procedure.

3.1. Effect of vertical seismic excitation on horizontal responses under different excitation conditions

3.1.1. Dynamic response of the structures

In this study, we investigate the dynamic response characteristics of girder bridge structures under near-field ground motion excitation. Given the significant differences in spectral characteristics and the mechanisms by which near-field and far-field ground motions affect structural dynamic responses, the structural responses induced by near-field motions are often more complex and severe. We first analyze the structural dynamic response under bidirectional excitation. A representative vertical-to-horizontal acceleration ratio of V/H=0.65, recommended by the Code for Seismic Design of Buildings (GB 50011-2010) [22], is adopted as the baseline case for subsequent analysis.

Figure 5 presents the dynamic responses of the bridge structure under seismic excitations with three characteristic periods of T=0.1 s, 0.2 s, and 0.5 s. Figure 5(a) shows the vertical displacement time histories at the girder mid-span and the pier top, and Figure 5(b) gives the corresponding horizontal displacement responses. For T=0.1 s and 0.5 s, the vertical displacement of the girder mid-span remains smaller than that of the pier top throughout the response process, indicating that no vertical separation occurs between the girder and the pier. In these cases, the contact constraint is maintained, and the structural dynamic characteristics remain essentially unchanged. Accordingly, the horizontal displacement responses obtained with and without vertical seismic excitation are almost the same. By contrast, when T=0.2 s, which is close to the first-order vertical natural period of the structure ($T_{1v}\approx$ 0.23 s), the vertical displacement at the girder mid-span exceeds that at the pier top on seven occasions, and the minimum vertical contact force decreases to zero ($F_{\min}$=0). These results indicate repeated loss of contact between the girder and the pier. The occurrence of vertical separation modifies the boundary constraint condition of the system and enhances the coupling between vertical and horizontal motions. As a consequence, the maximum horizontal relative displacement increases from 44.98 mm, when vertical excitation is neglected, to 77.15 mm when it is included. This shows that vertical seismic excitation may substantially amplify the horizontal response once contact loss is induced.

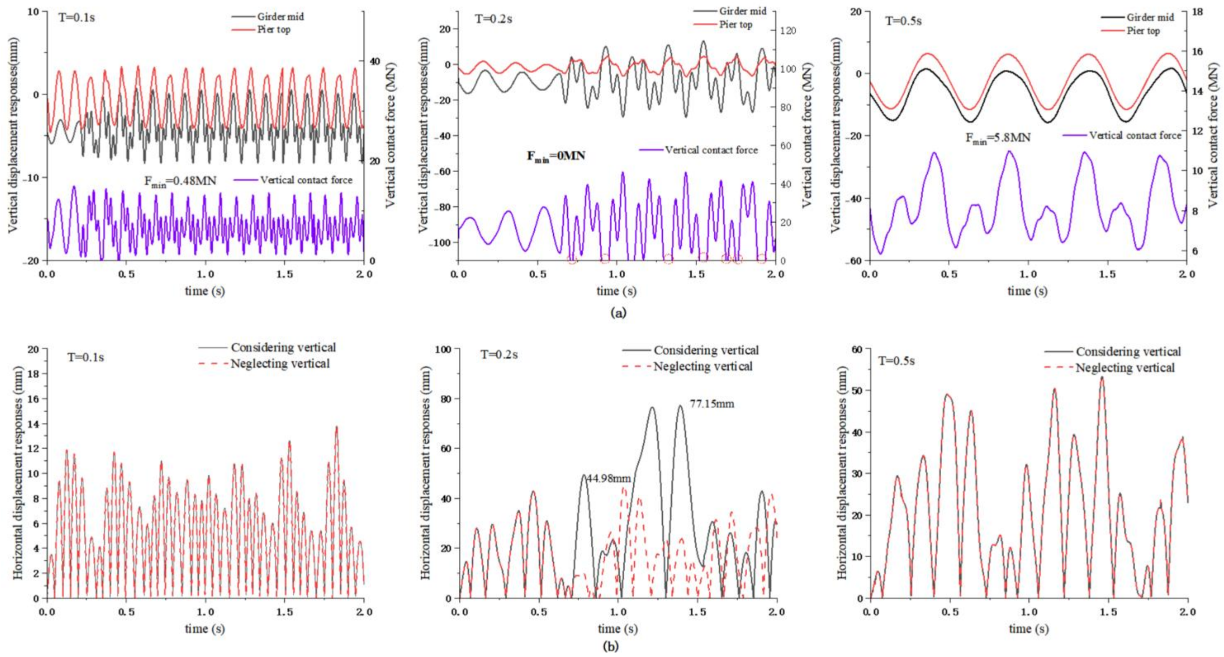

Figure 5. Time-history response of structures under bi-directional seismic excitation (a: Time-history of vertical seismic response at mid-span of girder and pier top; b: Time-history of horizontal seismic response at mid-span of girder and pier top).

3.1.2. Dynamic V/H values

Bridge seismic codes and research advancements reveal that the traditional seismic design framework, established primarily based on far-field ground motions, still fails to adequately account for the high-intensity characteristics of near-field ground motions, potentially leading to safety vulnerabilities in design. Consequently, adopting a fixed vertical-to-horizontal (V/H) spectral ratio of 0.65 likely underestimates the seismic damage sustained by bridges. It is therefore necessary to conduct a detailed analysis regarding the selection of the V/H ratio. Two models are employed: One based on the code-specified fixed V/H ratio of 0.65, and another based on the model proposed in [5], which features a dynamic V/H ratio in hard soil layers as shown in Eq (29).

$$\lambda = V / H = \begin{cases} \alpha & T < 0.1s \\ \alpha - \beta(T - 0.1) & 0.1s \leq T < 0.3s \\ 0.5 & T \geq 0.3s \end{cases} \tag{29}$$

where α is the peak value of the V/H ratio and β is the linear attenuation coefficient. In this study, the parameter values are selected according to the engineering background and seismic input conditions of the investigated bridge case. Considering the near-field scenario with an epicentral distance of 3 km, α is taken as 1.5 and β as 5. These values are used to characterize the relatively strong vertical component associated with the selected engineering case.

Figure 6 illustrates the bidirectional transient responses of the structure under fixed and dynamic V/H ratios. Compared with the fixed V/H ratio of 0.65, the dynamic V/H model yields a larger maximum vertical contact force, increasing from 46.1 MN to 50.6 MN, which indicates that the fixed V/H assumption may underestimate the vertical dynamic demand. The same tendency is observed in the horizontal response: The maximum relative displacement between the girder and the shear key reaches 113.8 mm under the dynamic V/H ratio, equal to 1.48 times that under the fixed V/H condition. This amplification is mainly caused by the stronger vertical excitation associated with the dynamic V/H model, which promotes girder uplift and reduces the effective lateral restraint of the bearings.

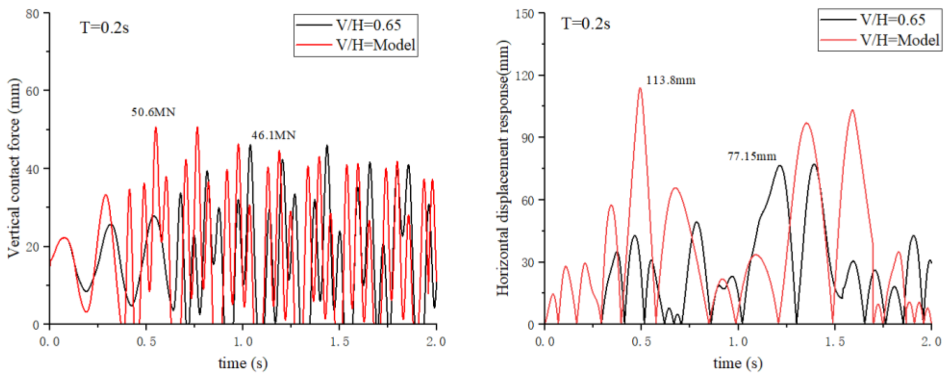

Figure 6. Bidirectional response of bridge structures under fixed and dynamic V/H excitation.

Furthermore, Figure 7 illustrates the influence of the two V/H values, corresponding to the fixed V/H ratio and the dynamic V/H model, on the horizontal dynamic response of the structure over a range of excitation periods. The results show that the overall variation trends of the peak horizontal displacement obtained from the two approaches are generally similar, and both reach their maximum values at T=0.3 s. At this excitation period, the input period is close to the first-order horizontal natural period of the structure, indicating a pronounced resonance effect. For T<0.3 s, the peak horizontal displacement predicted by the dynamic V/H model is consistently larger than that obtained using the fixed V/H ratio. This is mainly because, in the short-period range, the dynamic V/H model yields a relatively larger vertical seismic input, which intensifies the coupling effect between the vertical and horizontal responses. In addition, the stronger vertical excitation increases the likelihood of vertical separation between the girder and the bearings, thereby further amplifying the horizontal relative displacement. In contrast, when $T \geq 0.3$s, the influence of vertical excitation on the structural response becomes less significant, and the peak horizontal displacement calculated using the fixed V/H ratio becomes slightly larger. Overall, within the parameter range considered in this study, the dynamic V/H model has a more adverse effect on girder bridge structures in the short-period range, where the stronger vertical input may trigger more pronounced separation and consequently lead to greater seismic demand and potentially more severe structural damage.

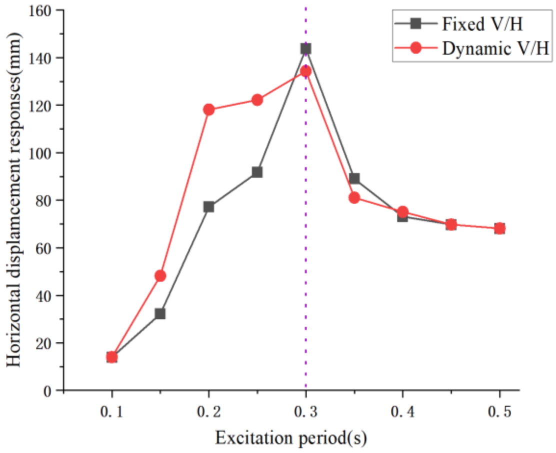

Figure 7. Horizontal dynamic response of the structure under fixed and dynamic V/H ratios at different excitation periods.

3.1.3. Different arrival times of seismic waves

Another important parameter characterizing near-field ground motions is the arrival-time difference between the bidirectional seismic wave peaks. Specifically, the peak of the vertical ground motion generally arrives earlier than that of the horizontal ground motion, resulting in a time interval between the two. To investigate the influence of this time interval, t_{cr}, on the structural dynamic response, Figure 8 (a) presents the results for three cases, namely t_{cr}=0 s, 0.1 s, and 0.15 s. The results indicate that, compared with the synchronous excitation case (t_{cr}=0 s), the horizontal relative displacements reach 107.12 mm and 116.19 mm when t_{cr}= 0.1 s and 0.15 s, respectively. This suggests that the arrival-time difference between the bidirectional seismic peaks affects the horizontal displacement response of the structure. Furthermore, Figure 8(b) compares the maximum horizontal relative displacements under different time-interval conditions. The results show that different arrival-time differences do cause variations in the horizontal structural response; however, the fluctuations remain within the range of $2d_{max}$ to $2.5d_{max}$ (d_{max} is the maximum horizontal displacement under neglected vertical excitation), without leading to unbounded displacement growth or abrupt changes. Therefore, it can be concluded that, within the parameter range considered in this study, the arrival-time difference has a certain influence on the peak horizontal displacement, although the overall effect is not significant.

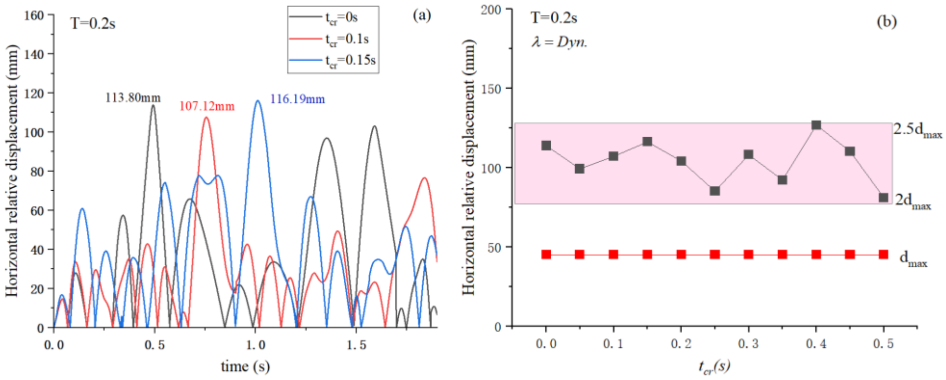

Figure 8. Horizontal dynamic response of structures under the influence of different time intervals (a: horizontal dynamic response; b: variation of maximum horizontal dynamic response).

3.1.4. The effect of different girder spans

To comprehensively evaluate the influence of near-field ground motions on girder bridges with different span lengths, we consider bridges with spans ranging from L=20 to 50 m. A dynamic model is adopted for horizontal and vertical seismic excitations. Since the previous results indicate that the effect of the arrival-time difference between bidirectional ground motions on the structural response is relatively limited, the vertical and horizontal ground motions are assumed to arrive simultaneously in the subsequent analyses. Figure 9 presents the horizontal dynamic responses of bridge structures with span lengths of L=30 m and L=50 m at T=0.2 s. For the bridge with L=30 m, the maximum relative displacement is 49.1mm. When the span increases to L=50 m, the fluctuation of the relative displacement becomes significantly more pronounced, and the maximum relative displacement reaches 134.2 mm. These results indicate that the horizontal displacement response of the structure tends to increase with increasing bridge span.

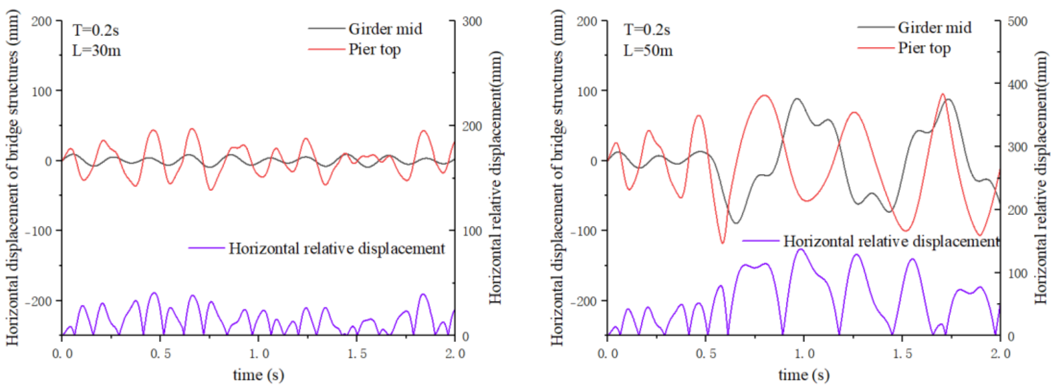

Figure 9. Horizontal dynamic response of the bridge for L=30m and L=50m.

Figure 10 compares the variation trends of the peak horizontal responses of girder bridges with different span lengths under two conditions: With and without consideration of vertical seismic excitation. Owing to the vertical separation effect induced by vertical ground motion, the horizontal dynamic displacement responses under the two conditions begin to show a pronounced difference when the span reaches L=30 m. In general, the horizontal dynamic response of the structure increases with increasing span length. However, when only horizontal seismic excitation is considered, the horizontal displacement response reaches its maximum at L=40 m and then gradually decreases. This phenomenon can be attributed to the fact that, at this span, the fundamental horizontal natural period of the structure approaches the dominant period of the input ground motion, thereby triggering a significant resonance effect and sharply amplifying the displacement response. The results indicate that, under near-field ground motions, an increase in span length may intensify the horizontal displacement response of girder bridges. Therefore, for long-span girder bridges, the coupling effect between the vertical and horizontal components of near-field ground motions should be carefully evaluated in seismic design so as to effectively mitigate their adverse effects.

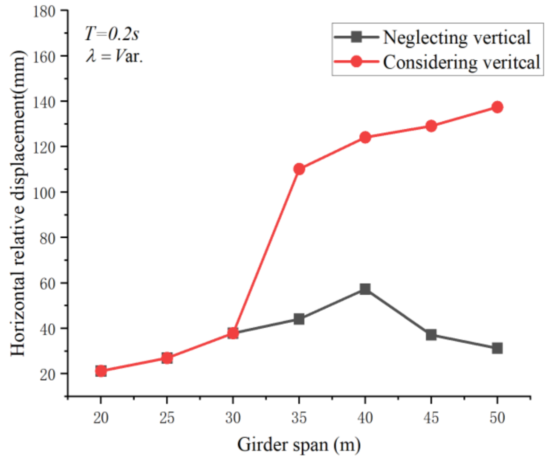

Figure 10. Horizontal dynamic response of the structure under different span lengths with and without considering vertical excitation.

3.2. Influence of near-field seismic excitation on the bridge substructure

Beyond global displacement responses, seismic response analysis can also be linked to safety-oriented threshold indicators. For instance, Zhai et al. proposed an efficient strong-seismic analysis model to evaluate running safety thresholds of a train–track–high-pier bridge dynamic system, highlighting the significance of threshold-based safety assessment in complex bridge-related systems [23]. Following this idea, in this section, we evaluate the contact–separation-induced amplification effect using local demand–capacity indicators for the pier base and shear key.

3.2.1. Bridge pier base flexural demand-capacity dynamics

The influence of contact–separation dynamics on the bridge pier response is further examined through the evolution of the normalized flexural demand at the pier base. Instead of directly evaluating structural failure, our analysis introduces the bending demand–capacity ratio:

$$DCR_{\mathrm{m}}(t) = \frac{|M(0,t)|}{M_u} \tag{30}$$

where M (0, t) denotes the transient bending moment at the pier base and M_u represents the nominal flexural capacity of the pier section.

Under this simplified framework, only the horizontal-response amplification induced by vertical separation is retained in the evaluation of $M(t)$. The secondary P–δ effect and the local impact effect associated with bearing re-contact are neglected. Consequently, the resulting *DCRm* should be interpreted as a reduced-order indicator characterizing the dominant amplification mechanism induced by the contact–separation transition. The transient bending moment M (0, t) at the pier base is shown as follows:

$$M(0,t) = \begin{cases} E_c I_c \dfrac{\partial X_c^2(\xi,t)}{\partial t^2}\Big|_{\xi=0}, & Contact\ \ state \\ E_c I_c \dfrac{\partial \bar{X}_c^2(\xi,t)}{\partial t^2}\Big|_{\xi=0}, & Separation\ \ state \end{cases} \tag{31}$$

where X_c and $\bar{X}_c$ are the dynamic responses of the pier during the contact and separation periods, respectively.

The bearing capacity is given by Eq (32):

$$M_{\mathrm{u}} \le \frac{2}{3} f_c A r \frac{\sin^3 \pi\alpha}{\pi} + f_y A_s r_s \frac{\sin \pi\alpha + \sin \pi\alpha_1}{\pi} \tag{32}$$

where A and r are the area and radius of the circular section; A_s and r_s denote the total longitudinal reinforcement area and its centroid radius; M_u is the nominal flexural capacity; and $\alpha$and $\alpha_1$are the normalized compression-zone angle and tensile-reinforcement ratio, respectively.

Based on the above formulation, the time-history response of the pier-base bending moment is calculated under different excitation periods, as shown in Figure 11. The results indicate that the flexural demand increases progressively as the excitation period becomes longer. In particular, the peak bending moment reaches M = 8.38MN at T = 0.25s, corresponding to DCR_m=1.73. Since this excitation period is close to the first vertical natural period of the coupled system ($T_{1v} \approx 0.23$ s), the observed amplification is likely associated with a resonance-like interaction between the vertical excitation and the contact–separation switching dynamics. Moreover, once the unilateral contact constraint is released, the coupled system exhibits enhanced horizontal modal interaction, resulting in a substantial increase in the normalized flexural demand at the pier base. The exceedance of the critical threshold DCR_m=1 indicates that the state-switching mechanism drives the structural response into a dynamically amplified regime dominated by nonlinear contact effects. Under this simplified framework, the pronounced increase in DCR_m suggests that the vertical separation effect acts as an effective nonlinear excitation mechanism capable of significantly amplifying the pier-base flexural demand.

Furthermore, Figure 12 compares the peak normalized flexural demand ratio at the pier base under excitation conditions with and without vertical ground motion. The results indicate that the peak value of DCR_m increases approximately monotonically with increasing excitation amplitude in both cases. However, when vertical seismic excitation is incorporated, the resulting DCR_m becomes consistently larger than that obtained without considering vertical ground motion, indicating a substantial amplification of the normalized flexural demand induced by vertical-contact dynamics. In particular, when the excitation period approaches the first vertical natural period of the coupled system, the peak response reaches a significantly amplified state. This amplification suggests that vertical excitation and contact–separation switching interact in a resonance-like manner. The release of the unilateral contact constraint changes the effective boundary conditions, enhances horizontal modal interaction, and consequently increases the normalized flexural demand at the pier base.

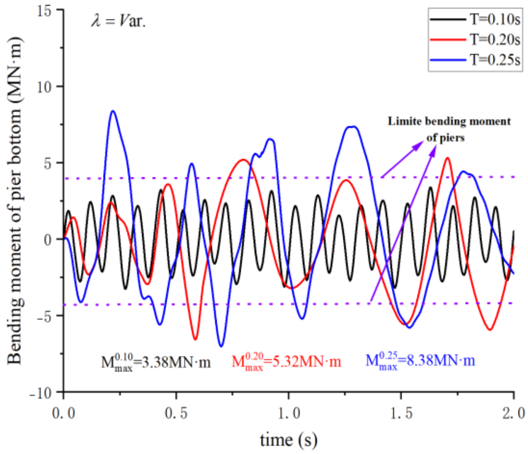

Figure 11. Dynamic bending moment response at the pier base under various excitation periods.

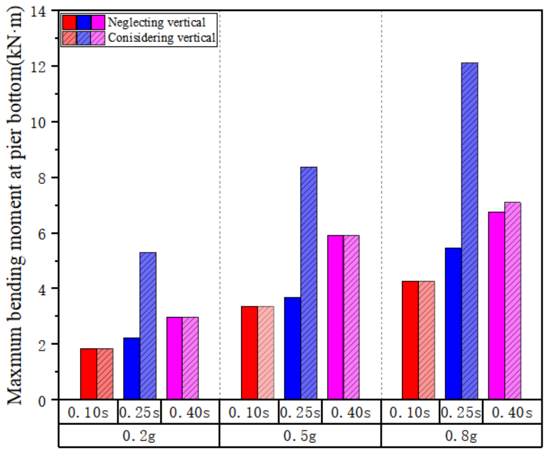

Figure 12. Effect of considered and neglected vertical excitation on the bending moment at the pier base under different excitation conditions.

3.2.2. Shear-key collision demand–capacity dynamics

The influence of contact–separation dynamics on the shear-key response is further examined through the normalized impact demand–capacity ratio. Instead of directly treating the shear-key failure as a deterministic event, this analysis introduces a reduced-order impact-risk indicator, defined as:

$$DCR_V(t) = \frac{|F_{col}(t)|}{V_n} \tag{33}$$

where $F_{\mathrm{col}}(t)$ denotes the transient horizontal collision force acting on the shear key, and V_{n} represents the nominal shear-friction capacity of the shear key.

When horizontal collision occurs, the following interface displacement condition is satisfied:

$$X_b\left(0,t_k\right)-X_c\left(H,t_k\right)-d\geq 0 \tag{34}$$

where $X_{\mathrm{b}}(0, t_{\mathrm{k}})$ and $X_{\mathrm{c}}(H,t_{\mathrm{k}})$ denote the displacement responses at the mid-span of the girder and the top of the pier, respectively, under contact or separation states. t_{k} denotes the occurrence time of the k-th collision event, with k=1,2, 3….

The transient horizontal collision force can be evaluated using the Duhamel integral in conjunction with the impulse response function. To avoid the computational difficulty associated with solving strongly nonlinear impact equations, a convolution integral approach is adopted to describe the displacement response induced by external excitation. Accordingly, the total displacement during the collision process can be expressed as the superposition of the pre-impact displacement X_{c} and the additional displacement induced by the collision response, which can be written as:

$$\begin{aligned} X_b^F &= X_b(0,t)+X_{bF}(0,t) \\ X_c^F &= X_c(H,t)+X_{cF}(H,t) \end{aligned} \tag{35}$$

where X_b^F, X_c^F represents the total displacement response of the girder–pier system during the collision process, and X_{bF}, X_{cF} denotes the additional displacement induced by the collision force.

Taking the horizontal collision during the separation phase as an example, the response can be described using the impulse response function and follows the corresponding impulsive excitation form:

$$\begin{aligned} X_{bF}(0,t) &= -\sum_{i=1}^{\infty}\varphi_{ib}(0)\int_0^{t_k^*}F_{col}(t_k+\tau)\frac{1}{m_{ib}\omega_{ib}}\sin\omega_{ib}(t-\tau)d\tau \\ X_{cF}(H,t) &= -\sum_{i=1}^{\infty}\varphi_{ic}(H)\int_0^{t_k^*}F_{col}(t_k+\tau)\frac{1}{m_{ic}\omega_{ic}}\sin\omega_{ic}(t-\tau)d\tau \end{aligned} \tag{36}$$

where t_k^* denotes the duration of the k-th collision process and satisfies $t_k^*=t-t_k$.

The collision force is obtained by enforcing the displacement compatibility condition at the shear-key interface, which converts the convolution expression into an integral equation for $F_{\mathrm{col}}(t)=K_{\mathrm{p}}\,[X_{\mathrm{bF}}(0, t)-X_{\mathrm{cF}}(H, t)]$.

For monolithic concrete shear keys, the nominal shear-friction capacity can be evaluated as:

$$V_N=\mu(A_{vf}f_{vf}+A_{vs}f_{vs}) \tag{37}$$

where μ is the friction coefficient, A_{vf} and f_{vf} denote the area and yield strength of the vertical reinforcement crossing the shear plane, respectively, and A_{vs} and f_{ys} denote the area and yield strength of the vertical reinforcement crossing the interface between the shear-key base and the adjacent components.

Figure 13 presents the time-history responses of the relative displacement and collision force of the bridge structure at T=0.2 s. It can be observed that t=0.472 s, horizontal relative displacement exceeds the initial clearance between the girder and the shear key, indicating the onset of collision. The collision force then increases rapidly and reaches a peak value of 3.94 MN. Subsequently, the force gradually decreases, and separation between the girder and the shear key occurs at t=0.518 s, marking the end of the collision process.

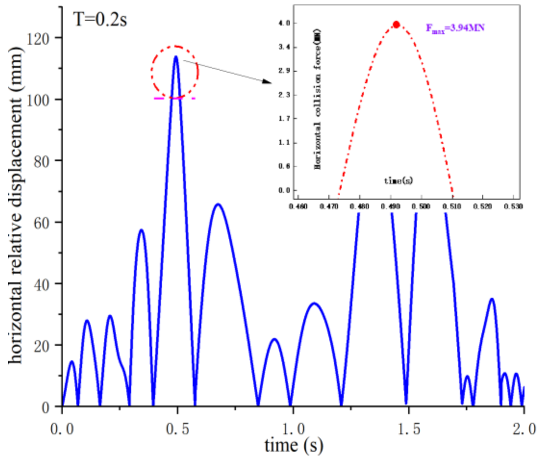

Figure 13. Calculation of the horizontal collision force time history for the structure at T=0.2s.

Figure 14 compares the peak collision forces under different excitation periods, with and without considering vertical ground motion. The maximum impact force occurs at T=0.25s, indicating that this excitation period represents the most unfavorable condition for shear-key impact within the considered parameter range. In contrast, the impact response remains relatively small at other excitation periods, such as T=0.1s and T=0.4s. This behavior can be attributed to the fact that, when the excitation period approaches the first vertical natural period of the structure, vertical vibration is significantly amplified and may trigger separation between the girder and the bearing. The resulting boundary-condition switching further increases the horizontal relative displacement and consequently amplifies the shear-key impact force.

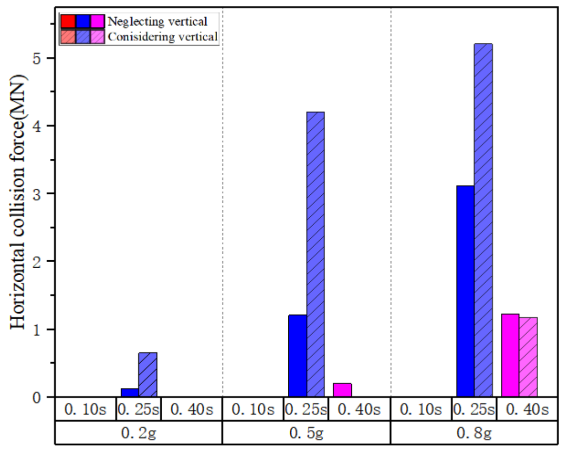

Figure 14. Influence of considered and neglected vertical excitation on the collision force of shear keys under different excitation conditions.

The magnitude of collision force alone is insufficient to assess structural safety. Figure 15 compares the peak horizontal collision force of the shear key with its nominal shear-friction capacity under different seismic excitation intensities. The results show that the collision force increases significantly with increasing excitation amplitude. When vertical ground motion is considered, the peak collision force is consistently larger than that obtained by neglecting vertical excitation, and the capacity threshold is reached at a lower excitation level. In particular, when the seismic excitation amplitude reaches approximately 0.4g, the peak collision force exceeds the nominal shear-friction capacity of the shear key, indicating that the shear key enters a potential capacity-exceedance state. In terms of the normalized demand–capacity ratio, this condition corresponds to $DCR_{SK}^{max}>1$. By contrast, when vertical excitation is neglected, the collision force remains below the nominal capacity over a wider range of excitation intensities, and capacity exceedance occurs only under stronger excitation. These results indicate that vertical excitation can significantly amplify the shear-key impact demand through the contact–separation mechanism. The comparison between collision force and shear capacity in Figure 15 directly shows the possible exceedance of the shear-key capacity, while DCR_{SK}^{max} provides a normalized auxiliary indicator for quantifying this phenomenon. Therefore, neglecting vertical ground motion may lead to a non-conservative evaluation of shear-key safety in girder bridges subjected to near-field bidirectional seismic excitation.

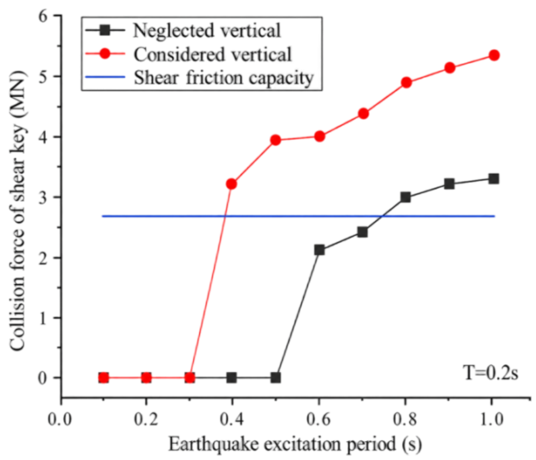

Figure 15. Comparison between peak shear-key collision force and nominal shear-friction capacity under different excitation intensities at $T = 0.2$ s.

4. Finite element verification of the analytical model

To further verify the proposed theoretical formulation, a simplified finite element (FE) model is established in OpenSees. The geometric dimensions, material properties, bearing stiffness, and excitation parameters are kept consistent with those used in the analytical model. The girder and central pier are modeled using elastic beam-column elements, with hinged constraints at both girder ends and a fixed constraint at the pier base. The girder–pier bearing interface is simulated using zero-length elements: Kelvin–Voigt Spring with 2% viscous damping is adopted in the horizontal X-direction, while a linear elastic spring is used in the vertical Z-direction. The simplified FE model is shown in Figure 16.

Figure 17 compares the pier-top horizontal displacement responses obtained from the OpenSees FE model and the proposed theoretical analytical model (referred to as the analytical model below). The two models exhibit generally consistent response trends under the three excitation periods. For

T=0.1 s, the displacement amplitude is relatively small, and the agreement between the two results is satisfactory. When the excitation period increases to T=0.2 s and T=0.4 s, the pier-top displacement is significantly amplified, and both models capture the increase in response amplitude. Although slight phase differences and local peak discrepancies are observed, especially for larger-amplitude responses, the overall displacement envelopes remain comparable. These differences are mainly attributed to the idealized continuous formulation adopted in the analytical model and the discretized beam-spring representation used in the OpenSees model. Therefore, the comparison confirms that the proposed analytical model can reasonably reproduce the major horizontal dynamic response characteristics of the pier top under harmonic excitation. To further quantify the agreement between the analytical model and the OpenSees FE model, the peak horizontal displacement responses at the pier top are compared under different excitation periods. The relative error is calculated using the analytical result as the reference value. The comparison results are summarized in Table 1.

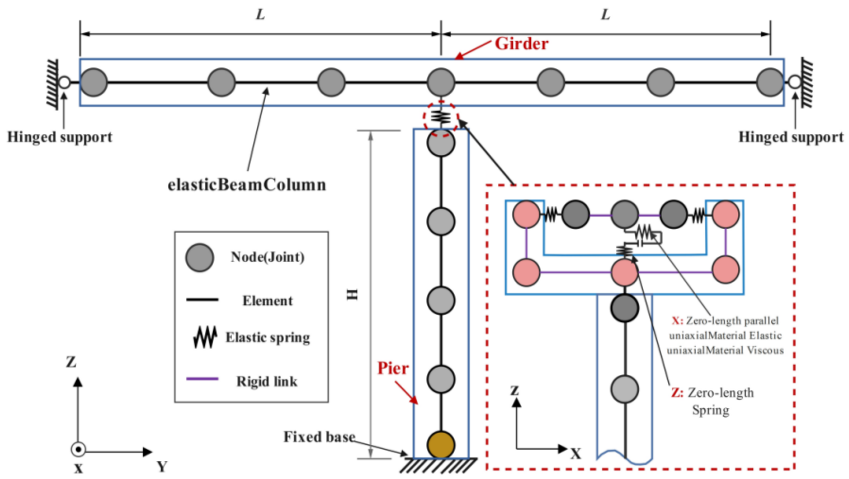

Figure 16. The OpenSees FE model and bearing configuration of the two-span girder bridge.

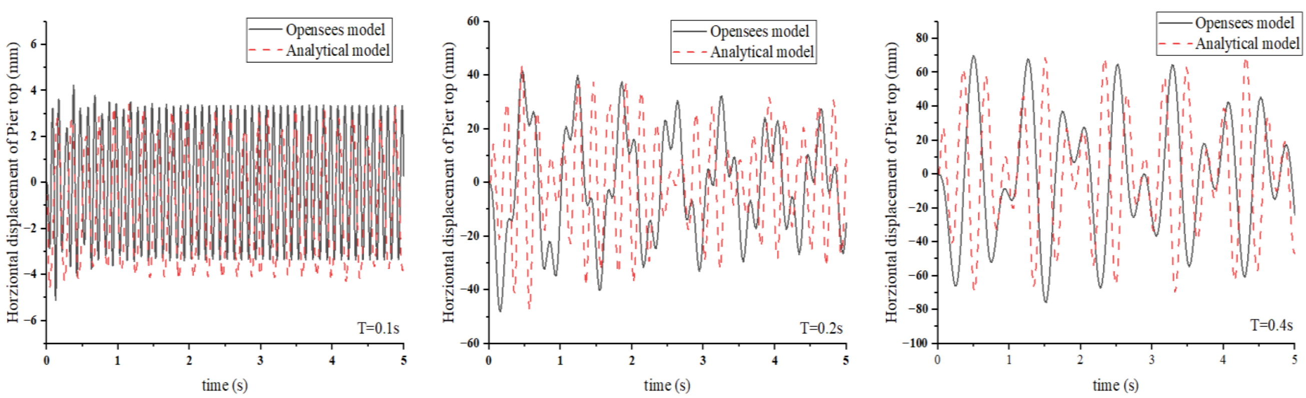

Figure 17. The pier-top horizontal displacement responses predicted by the OpenSees FE model and the analytical model.

Table 1. Quantitative comparison of pier-top peak horizontal displacement responses between the analytical and OpenSees models.

Excitation period (s)	Analytical peak (mm)	OpenSees peak (mm)	Relative error (%)
T=0.1s	4.68	5.10	≈8.97%
T=0.2s	47.40	49.19	≈3.77%
T=0.4s	69.62	75.54	≈8.50%

Furthermore, the peak pier-top displacements obtained from the analytical and OpenSees models are compared in Table 1. The relative errors are approximately 8.97%, 3.77%, and 8.50% for T=0.1 s, 0.2 s and 0.4 s, respectively, all of which are less than 10%. The OpenSees model predicts slightly larger peak responses in all cases, which may be attributed to differences in spatial discretization, boundary-condition implementation, and damping representation. The slight phase differences and local peak discrepancies are mainly caused by differences in modeling strategy. The analytical model idealizes the girder–pier system as a continuous beam-type system and uses a limited number of retained modes, whereas the OpenSees model adopts a discretized beam–spring representation with finite-element-based boundary constraints and zero-length bearing elements. In addition, the simplified contact–separation treatment in the analytical model may not fully capture local high-frequency re-contact effects. Nevertheless, these discrepancies are acceptable for a reduced-order analytical model, and the quantitative comparison confirms that the proposed formulation can reasonably capture the dominant horizontal response trend and amplitude.

5. Conclusions

A state-switching PDE model was developed to investigate contact–separation-induced response amplification in girder bridges subjected to bidirectional seismic excitation. The vertical girder–bearing interaction was formulated using a unilateral contact condition, which governs the transition between contact and separation states. Accordingly, the horizontal transient response was described by state-dependent beam-type PDEs with switching boundary conditions. Based on our theoretical formulation and numerical results, the following conclusions can be drawn:

(1) The proposed formulation shows that the essential transient mechanism is the state transition induced by vertical excitation. When the girder remains in continuous contact with the bearing, the influence of vertical excitation on the horizontal response is limited. However, when the excitation period approaches the first vertical natural period of the structure, repeated contact loss occurs and causes boundary-condition switching, which significantly amplifies the horizontal transient response.

(2) Within this PDE-based framework, the V/H ratio and bridge span are identified as the major parameters governing the amplification effect under bi-directional excitation. Compared with the conventional fixed V/H assumption, the dynamic V/H model leads to a more adverse response, especially in the short-period range, whereas the arrival-time difference between the vertical and horizontal seismic peaks has only a limited influence within the parameter range considered. Increasing span length further enhances the amplification associated with contact–separation behavior.

(3) The contact–separation-induced amplification is not limited to the global horizontal displacement response as it also increases local demand–capacity indicators. When vertical excitation is considered, the pier-base flexural demand–capacity ratio, DCR_M , increases significantly, indicating that the flexural demand of the bridge substructure may be underestimated if vertical ground motion is neglected. Similarly, the shear-key collision force reaches the nominal shear-friction capacity at a lower excitation level, and the corresponding capacity-exceedance condition can be expressed as $DCR_v^{\max}>1$. These results demonstrate that vertical excitation may increase the flexural demand of the pier base and the impact-risk level of the shear key.

(4) The FE comparison further confirms that the proposed analytical model can reasonably reproduce the major horizontal dynamic response characteristics of the girder–pier system. The OpenSees results and the analytical solutions show generally consistent displacement trends and comparable response envelopes under harmonic excitation, although slight phase differences and local peak discrepancies are observed due to different modeling strategies. Overall, the proposed state-switching PDE model provides an effective reduced-order framework for describing the coupling among unilateral contact, boundary-condition evolution, and transient response amplification.

Although the proposed state-switching PDE model provides a useful reduced-order framework for describing contact–separation-induced response amplification, further extensions may improve its applicability to more realistic bridge systems. Future work may include scaled shaking-table tests to experimentally validate the state-switching mechanism, incorporation of soil–structure interaction through flexible foundation boundary conditions, and extension of this formulation to account for material nonlinearity, such as pier plastic hinge formation and stiffness degradation under severe earthquakes. In addition, the model can be further examined using a broader set of real seismic records, including near-fault pulse-like motions and long-duration far-field earthquakes, to evaluate its robustness under different excitation characteristics.

Author contributions

Shutong Chen: Conceptualization, Methodology; Jieqin Liu and Leilei Li: Investigation, Writing original draft; Xuerong Liu and Fuxing Ding: Resource, Formal analysis. All authors have read and approved the final version of the manuscript for publication.

Use of Generative-AI tools declaration

The authors declare they have used Artificial Intelligence (AI) tools in the creation of this article.

Acknowledgments

The authors gratefully acknowledge the valuable support and constructive suggestions received during the preparation of this study. This work was supported by the Science and Technology Project of Jiangxi Provincial Department of Education, China (Grant No. GJJ2402901), the Corporate Collaborative Project of Jiangxi Polytechnic Institute, China (Grant No. 2025-JGHX-28), and the Teaching Reform Project of Jiangxi Polytechnic Institute, China (Grant No. 2024-JGJG-64).

Conflict of interest

The authors declare that they have no known competing financial interests or personal relationships that could have appeared to influence the work reported in this paper.

References

1. D. K. Keefer, Statistical analysis of an earthquake-induced landslide distribution–the 1989 Loma Prieta, California event, *Eng. Geol.*, **58** (2000), 231–249. https://doi.org/10.1016/S0013-7952(00)00037-5
2. Y. Fukushima, K. Irikura, T. Uetake, H. Matsumoto, Characteristics of observed peak amplitude for strong ground motion from the 1995 Hyogoken Nanbu (Kobe) earthquake, *Bull. Seismol. Soc. Amer.*, **90** (2000), 545–565. https://doi.org/10.1785/0119990066
3. S. W. Geng, X. X. Tao, The ratios of vertical to horizontal acceleration response spectra, *Earthq. Eng. Eng. Vib.*, **24** (2004), 33–38. https://doi.org/10.3969/j.issn.1000-1301.2004.05.007
4. Y. Bozorgnia, K. W. Campbell, *Vertical Ground Motion: Characteristics, Modeling, and Applications in Seismic Design*; California: University of California: Berkeley, 2004.
5. Y. Bozorgnia, K. W. Campbell, The vertical-to-horizontal response spectral ratio and tentative procedures for developing simplified V/H and vertical design spectra, *Earthq. Eng. Eng. Vib.*, **8** (2004), 175–207. https://doi.org/10.1080/13632460409350486
6. K. H. Luo, K. W. Yang, Research and application progress of vertical seismic response spectrum, *J. Civil*, *Architect. Environ. Eng.*, **32** (2010), 198–201.
7. A. J. Papazoglou, A. S. Elnashai, Analytical and field evidence of the damaging effect of vertical earthquake ground motion, *Earthq. Eng. Struct. Dyn.*, **25** (1996), 1109–1137. https://doi.org/10.1002/(SICI)1096-9845(199610)25:10<1109::AID-EQE604>3.0.CO;2-0
8. K. Bi, H. Hong, N. Chow, Required separation distance between decks and at abutments of bridge crossing a canyon site to avoid seismic pounding, *Earthq. Eng. Struct. Dyn.*, **39** (2010), 303–323. https://doi.org/10.1002/eqe.943
9. S. Tanimura, H. Heya, T. Umeda, K. Mimura, O. Yoshikawa, 3-Dimensional analysis of dynamic behavior of bearing of Nielsen bridge, *JSME Int. J*, **2** (2002), 190–198. https://doi.org/10.1299/jsmea.45.190
10. C. J. Wang, M. H. Shih, Performance study of a bridge involving sliding decks and pounded abutment during a violent earthquake, *Eng. Struct.*, **29** (2007), 802–812. https://doi.org/10.1016/j.engstruct.2006.05.026
11. N. Chouw, H. Hao, Pounding damage to buildings and bridges in the 22 February 2011 Christchurch Earthquake, *Int. J. Prot. Struct.*, **3** (2011), 123–139. https://doi.org/10.1260/2041-4196.3.2.123
12. A. C. Eringen, E. S. Suhubi, *Elastodynamics*, New York: Academic Press, 1975.
13. B D. St.venant, M. Flamant, Résistance vive ou dynamique des solids, *Resprésentation Graphique Longitudinal*, **97** (1883), 127–353.
14. S. Timoshenko, D. H. Young, W. J. R. Weaver, *Vibration Problems in Engineering*, New York: John Wiley and Sons, 1974.
15. A. Tian, X. Yin, Transient dynamics analysis for multiple-impact of flexible-rods, in Chinese, *Chin. J. Mech. Eng.*, **44** (2008), 43–48.

16. R. Xu, X. C. Yin, Transient wave response analysis of a bridge under vertical earthquakes, *J. Vibr. Shock*, **31** (2012), 49–55.
17. R. Xu, X. C. Yin, Calculations of multiple pounding forces between girder and pier of bridges under vertical earthquakes, *Eng. Mech.*, **27** (2010), 124–130.
18. H. B. Yang, X. C. Yin, R. Xu, Effect of bridge bearings on vertical pounding in bridges under near-fault vertical earthquake, *Eng. Mech.*, **31** (2014), 183–189. https://doi.org/10.1002/eqe.2601
19. H. B. Yang, X. C. Yin, Transient responses of girder bridges with vertical poundings under near-fault vertical earthquake, *Earthq. Eng. Struct. Dyn.*, **44** (2015), 2647–2657. https://doi.org/10.6052/j.issn.1000-4750.2012.12.1020
20. W. J. An, L. Zhou, M. Kang, H. L. Yang, L.Y. Mo, Failure mode analysis of bridge pier due to eccentric impact based on separation of pier and beam, *Sustainability*, **2** (2023), 1435. https://doi.org/10.3390/su15021435
21. W. An, P. Zhou, P. Wang, Z. Zheng, H. Yang, Analysis of dynamic interaction and response in multispan girder bridges subjected to near-fault earthquakes, *Structures*, **58** (2023), 105622. https://doi.org/10.1016/j.istruc.2023.105622
22. Ministry of Housing and Urban-Rural Development of China. Code for Seismic Design of Buildings 2016, GB 50011-2010.
23. Z. Zhai, Y. Li, S. Zhu, C. Cai, An efficient strong seismic analysis model for running safety thresholds of train-track-high pier bridge dynamic system, *Eng. Struct.*, **357** (2026), 122476. https://doi.org/10.1016/j.engstruct.2026.12247622